Temperature-Induced Molten Globule-like State in Human α_1-Acid Glycoprotein: An Infrared Spectroscopic Study†

Alessio Ausili,‡ Andrea Scirè,‡ Elisabetta Damiani,* Giovanna Zolese, Enrico Bertoli, and Fabio Tanfani

Istituto di Biochimica, Università Politecnica delle Marche, Ancona, Italy

Received July 29, 2005; Revised Manuscript Received October 17, 2005

ABSTRACT: Despite extensive investigations on thermal denaturation of α_1-acid glycoprotein (AGP) using a variety of techniques, structural features of the folded−unfolded state in terms of residual secondary structures and the structural transitions involved in this process have not been fully characterized. In this study we employed FT-IR spectroscopy to investigate the thermal unfolding and reversibility of temperature-induced changes in AGP. The data revealed a fully reversible β-sheet-rich protein which exhibits a molten globule-like state, an important protein folding intermediate. 2D-IR COS revealed the sequence of the conformational changes occurring before denaturation and confirmed the formation of this intermediate which was further supported by CD spectroscopy. On account of the similarities in the FT-IR spectra of AGP with those of porcine odorant-binding protein (OBP), homology modeling of AGP using OBP as template was performed. The resemblance of AGP and OBP 3D structures confirmed the similarities of data obtained using FT-IR spectroscopy. Overall, FT-IR spectroscopy appears to be useful for investigating the structural characteristics and stability of proteins whose 3D structures are unavailable and for assessing the molten globule-like state in small β-sheet-rich proteins.

α_1-Acid glycoprotein (AGP), also known as orosomucoid, first described in 1950, is a much studied plasma glycoprotein (M_r = 41000) included in the lipocalin family (*1*). Until a few years ago, it was considered to be the protein with the highest carbohydrate content. Indeed, it contains 42% carbohydrate by weight and up to 16 sialic acid residues which are part of the five heteropolysaccharide groups attached via asparaginyl residues to the protein. These sialic acid residues contribute to the extremely low isoelectric point of AGP, which varies between pH 1.8 and pH 2.7 according to the buffer used, and are responsible for its high solubility and unusual stability in neutral solutions. Its 183 aa single polypeptide chain contains two disulfide bridges between cysteines 5−147 and 72−164 and three Trp residues: one at the surface of the protein and two located in the protein matrix (*2*−*4*).

The definitive biological role of AGP has not yet been elucidated despite the numerous studies devoted to it and its relatively high concentration in plasma (~70 mg/100 mL). Its hepatic production increases following the response to various stressful stimuli: physical trauma, bacterial infection, or unspecific inflammatory stimuli, hence its classification as a major member of the acute phase protein family (*3*). It also binds certain steroids (progesterone) and basic drugs (propanolol, vanilloids) in plasma that can have important pharmacokinetic implications (*5*−*7*). AGP is considered a natural antiinflammatory and immunomodulatory agent notably with respect to its antineutrophil and anticomplement activity, suggesting that this constitutively produced glycoprotein plays a crucial role in maintaining homeostasis (*8*, *9*). Now, for a clear understanding of the biological activity of any protein, it is fundamental to comprehend its structural characteristics and stability. For AGP, several experimental approaches have been used, especially since no crystallographic data describing its 3D structure are available. These include heat denaturation and isothermal, water-soluble organic solvent-induced denaturation studies using circular dichroism (CD), fluorescence, UV absorbance difference, and Raman spectroscopies, as well as differential scanning calorimetry (*10*−*15*). Each method represents a different way of looking at the protein molecule. Surprisingly, there is only one report in the literature on the use, briefly, of FT-IR spectroscopy for studying this popular protein (*16*). FT-IR spectroscopy is a global, sensitive, and highly reproducible physicochemical analytical technique that identifies structural moieties of biomolecules on the basis of their IR absorption. In fact, it is a valuable method for studying protein denaturation because the frequencies, intensities, and bandwidths of characteristic bands in an IR spectrum of a protein are very sensitive to conformational changes in the protein and to the microenvironment. Therefore, this technique, combined with 2D-IR correlation analysis, was employed to investigate further and in detail the thermal stability and reversibility of temperature-induced changes of AGP at neutral pH. In addition, it was of interest to verify, using this experimental approach, whether AGP exhibits a multistate behavior upon thermal denaturation, as suggested by other investigators (*11*, *13*) and as previously observed by us on another member of the lipocalin family, the porcine odorant-binding protein (*17*).

† This work was supported by a grant from the Università Politecnica delle Marche (to F.T.).

* Corresponding author. Tel: +390712204318. Fax: +390712204398. E-mail: e.damiani@univpm.it.

‡ These authors contributed equally to this work.

10.1021/bi051512z CCC: $30.25
Published on Web 11/10/2005

MATERIALS AND METHODS

Materials. Human α_1-acid glycoprotein (AGP), deuterium oxide (99.9% ^2H_2O), ^2HCl, NaO^2H, Na_2HPO_4, and NaH_2PO_4 were purchased from Sigma-Aldrich. All other chemicals used were commercial samples of the purest quality.

Preparation of Samples for Infrared Measurements. For each sample, about 1.5 mg of protein was dissolved in 200 μL of 20 mM phosphate buffer, pH 7.4 or p^{2}H 7.4, and centrifuged in a "30 K Centricon" microconcentrator (Amicon) at 3000*g*, 4 °C, until the volume of the solution reached approximately 40 μL. Then, a further 200 μL of buffer was added, and the solution was reconcentrated. This procedure was repeated five times in order to completely hydrate the protein with the chosen buffer. The final concentration of the protein solution for analysis was approximately 3.0% (w/v). In total, the washings took 24 h, which is also the time of contact of the protein with the medium prior to FT-IR experiments. The p^{2}H value was measured with a standard pH electrode, and the value was corrected according to p^{2}H = pH + 0.4 (*18*).

Infrared Spectra. The concentrated protein sample was injected into a thermostated Graseby Specac 20500 cell (Graseby-Specac Ltd., Orpington, Kent, U.K.) fitted with CaF_2 windows and a 6 μm tin spacer or a 25 μm Teflon spacer for the experiments in ^1H_2O or ^2H_2O, respectively. FT-IR spectra were recorded by means of a Perkin-Elmer 1760-x Fourier transform infrared spectrometer using a deuterated triglycine sulfate detector and a normal Beer−Norton apodization function. At least 24 h before, and during data acquisition, the spectrometer was continuously purged with dry air at a dew point of −40 °C. In the thermal unfolding and refolding experiments an external bath circulator (HAAKE F3) was used, and spectra were collected every 5 °C in the 20−90 °C temperature range. The actual temperature in the cell was controlled by a thermocouple placed directly onto the windows. Spectra of buffers and samples were acquired at 2 cm^{-1} resolution under the same scanning and temperature conditions. Spectra were collected and processed using the SPECTRUM software from Perkin-Elmer. Correct subtraction of H_2O was judged to yield an approximately flat baseline at 1900−1400 cm^{-1}, and subtraction of ^2H_2O was adjusted to the removal of the ^2H_2O bending absorption close to 1220 cm^{-1} (*19*). The deconvoluted parameters were set with a γ value of 2.5 and a smoothing length of 60. Second derivative spectra were calculated over a nine data point range (9 cm^{-1}). $^1H/^2H$ exchange during thermal denaturation was checked by monitoring the intensity of the residual amide II band (*20*). The $T_{1/2}$ of the residual amide II band intensity was obtained, applying a sigmoidal fit to the experimental data (*21*). Estimation of the secondary structure composition was carried out by curve fitting of the deconvoluted amide I′ band (*22*) using the peak-fitting module included in the software OriginPro 7.5 (OriginLab Corp., Northampton, MA).

CD Spectra. Near-UV (from 310 to 250 nm) and far-UV CD spectra (from 260 to 200 nm) were recorded on a Jasco 500 spectropolarimeter under constant nitrogen flux at different temperatures. An external bath circulator (HAAKE F3) was used to maintain the desired temperature, and the actual temperature inside the cell was controlled by a thermocouple placed directly inside the cell holder. The instrument was calibrated with a solution of 0.015% pantolactone as previously described (*23*). Quartz cells of 0.1 or 1 cm path lengths were used in the far-UV and near-UV regions, respectively. The AGP concentration was 8 μM (far-UV) and 20 μM (near-UV) in 20 mM phosphate buffer, pH 7.4. For all spectra, an average of three scans was obtained. The CD spectrum of the buffer was recorded and subtracted from the protein spectra.

Two-Dimensional Infrared Correlation Analysis. Generalized 2D-IR correlation analysis of deconvoluted spectra of AGP, using heat as the perturbation, was performed as described by Noda (*24*). To obtain synchronous and asynchronous plots, 2Dshige (Shigeaki Morita, Kwansei-Gakuin University, 2004−2005) was used (*25*−*27*). Two sets of synchronous and asynchronous plots, covering 20−65 and 65−90 °C, were generated. These temperature ranges allowed us to better describe the thermal unfolding events (*28*).

Homology Modeling. The AGP 3D structure was obtained by submitting to ESyPred3D Web Server 1.0 the sequence of AGP using OBP (1A3Y) as template. When the sequence of AGP was previously submitted to Swiss Model, no matches were found; consequently, OBP was chosen as a template on the basis of the fact that its FT-IR spectral features and thermal behavior were identical to those of AGP (*17*), despite a result of only 15.8% identities in sequence alignment. In fact, both of these proteins belong to the same subgroup of the lipocalin family, the outlier lipocalins, where its members share pairwise sequence identity falling below 20%. ESyPred3D is a new automated homology modeling program. The method takes advantage of the increased alignment performances of a new alignment strategy using neural networks. Alignments are obtained by combining, weighting, and screening the results of several multiple alignment programs. The final three-dimensional structure is built using the modeling package MODELLER (*29*).

"Phase Diagram" Method of FT-IR and CD. The phase diagram method is a sensitive approach for the detection of unfolding/refolding intermediates of proteins (*30*). The essence of this method is to build up the diagram of $I(\lambda_1)$ versus $I(\lambda_2)$, where $I(\lambda_1)$ and $I(\lambda_2)$ are the FT-IR absorbance spectral intensity values measured on wavelengths λ_1 and λ_2 under different experimental conditions, in our case at different temperatures, for a protein undergoing structural transformations. With the change of denaturing factors such as temperature, the transitions from the initial to the final state follow a "two-state" or "all-or-none" model without formation of the intermediate states, so the dependence must be linear. If the transition from the initial to the final state follows a "three-state" or "multi-state" model with the formation of one or several intermediate states, the dependence $I(\lambda_1) = f(I(\lambda_2))$ must be nonlinear and must contain two or more linear portions. Each linear portion dependence will describe an individual all-or-none transition. The same method was applied to build up a phase diagram using the spectral ellipticity values from the CD spectra at two different wavelengths as reported by ref *30*.

RESULTS

FT-IR Spectra of AGP. Figure 1A shows typical Fourier transform infrared absorbance spectra measured on α_1-acid glycoprotein in ^1H_2O and ^2H_2O, in the region from 1750 to

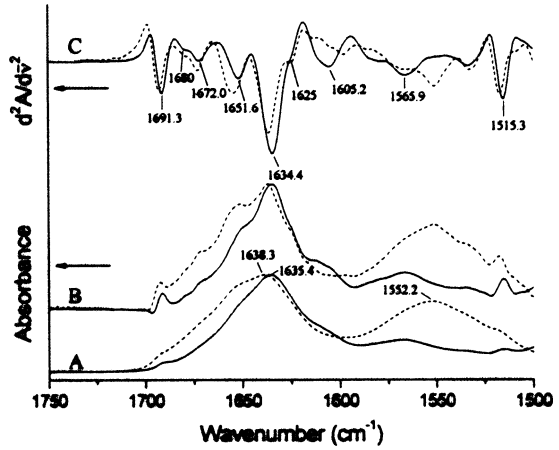

FIGURE 1: Original absorbance (A), deconvoluted (B), and second derivative (C) spectra of AGP at 20 °C, pH or p^{2}H 7.4. Continuous and dashed lines refer to spectra of AGP in ^2H_2O and ^1H_2O, respectively.

1500 cm^{-1}, after digital subtraction of the respective buffer spectra. In ^1H_2O (Figure 1A, dotted line), two prominent bands are visible: the amide I band centered at 1638.3 cm^{-1} and the amide II band centered at 1552.2 cm^{-1}. In ^2H_2O (Figure 1A, continuous line), due to the $^1H/^2H$ exchange of amide protons with deuterons, the amide I and the amide II bands shift to lower wavenumbers. The amide I band is now located at 1635.4 cm^{-1}, while the position of the amide II band, which is very sensitive to deuteration, moves to 1450 cm^{-1} (not shown). The shifting of the amide II band at 1450 cm^{-1} causes a large decrease in its intensity at 1550 cm^{-1}, a decrease that is a measure of the $^1H/^2H$ exchange. This remainder of the amide II band at 1550 cm^{-1} can be more or less intense, depending on the accessibility of the protein to the solvent, and is called the residual amide II band. The lower the intensity of the residual amide II band, the higher the accessibility of the protein (*20*, *31*, *32*). Since the residual amide II band is extremely low (Figure 1A, continuous line), AGP appears to be highly accessible to the solvent.

However, the most important band in conformational studies is the amide I band which is located between 1700 and 1600 cm^{-1}. The amide I band of proteins consists of a series of overlapped component bands which occur as a result of the secondary structures present in such molecules, and resolution enhancement of the absorbance spectra allows the identification of these structures (*33*, *34*). To obtain such information, the deconvoluted and the second derivative spectra of AGP are shown in panels B and C of Figure 1, respectively. In the amide I′ region, the deconvoluted and the second derivative spectra of AGP show six bands. The 1625, 1634.4, and 1691.3 cm^{-1} bands are characteristic of β-sheet structures. In particular, the 1625 cm^{-1} band may be attributed to the β-edge, i.e., β-strands particularly exposed to the solvent (*35*). The band at 1651.6 cm^{-1} is assigned to α-helix structure, while the 1672.0 and the 1680 cm^{-1} bands reveal the presence of turns and/or β-sheets/turns, respectively (*33*, *36*). The bands below 1620 cm^{-1} are due to absorptions deriving from certain amino acid side chains. In particular, the 1515.3 and the 1605.2 cm^{-1} bands are due to tyrosine and ionized hydroxyl residues of tyrosine, respectively, while the 1565.9 cm^{-1} band is due to ionized carboxyl groups of glutamic acid residues (*37*).

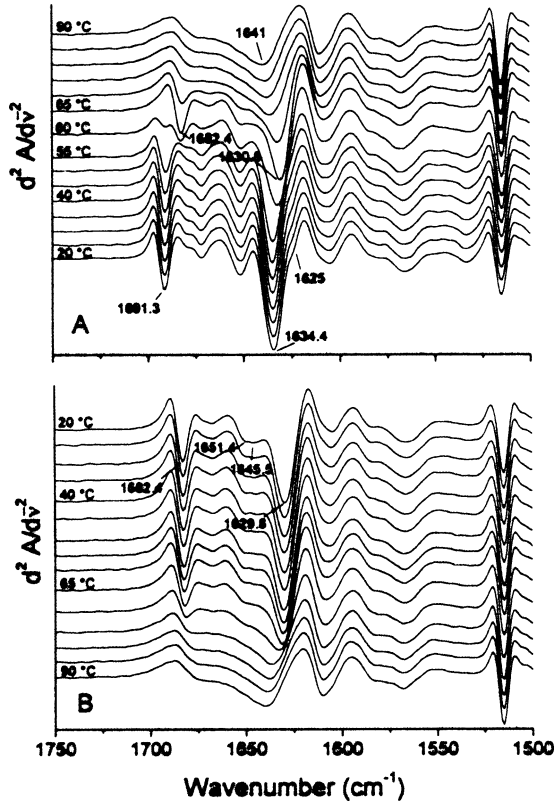

FIGURE 2: Second derivative spectra of AGP in the 20−90 °C (panel A) and 90−20 °C (panel B) temperature range. Second derivative spectra were calculated over a nine data point range (9 cm^{-1}) and displayed at 5 °C intervals.

Thermal Unfolding of AGP. The temperature-induced conformational changes of the protein can be monitored following the pattern of the spectral bands recorded at different temperatures. Figure 2A shows the second derivative spectra of AGP from 20 to 90 °C while Figure 2B shows those from 90 to 20 °C. In Figure 2A, one can observe that up to 50 °C the spectral bands remain practically identical except for the disappearance, on increasing temperature, of the shoulder at 1625 cm^{-1} assigned to β-edge structures, suggesting loosening of their intramolecular hydrogen bonds. Therefore, up to 50 °C the protein does not show any important conformational changes. Between 50 and 65 °C, spectral changes appear which mainly concern the β-sheet bands. In particular, the presence at 65 °C of a strong peak around 1630 cm^{-1} and of a weaker one around 1680 cm^{-1}, typical of the peptide bond in an antiparallel chain β-sheet conformation (*38*, *39*) previously located at 1634.4 cm^{-1} and at 1691.3 cm^{-1} at 20 °C, stands out. The exposure of these antiparallel chain β-sheets to the solvent, from 50 to 65 °C, leads to additional $^1H/^2H$ exchange of the protein as indicated by their downshift in wavenumber (the first, great $^1H/^2H$ exchange occurs during sample preparation in ^2H_2O; see also Figure 1). This is strongly supported by the fact that this particular secondary structure absorbs at a high frequency around 1690 cm^{-1} when it is in ^1H_2O while, when in ^2H_2O, the peak greatly shifts to around 1680 cm^{-1} (*38*, *39*). These changes are most likely due to relaxation of the tertiary structure induced by temperatures between 50 and 65 °C, which leads to solvent accessibility in the protein core. No significant decrease in band intensity was observed, indicating that, in this range of temperature, the protein maintains

its secondary structure despite its more relaxed state. Between 65 and 90 °C there is a progressive decrease in intensity of the peaks of the amide I′ region indicating loss of secondary structure elements caused by protein denaturation. At 90 °C the main peak is now centered at 1641 cm^{-1}, a frequency characteristic of unordered structures. AGP was then cooled stepwise from 90 to 20 °C (Figure 2B). The figure shows that from the denatured state at 90 °C the protein progressively refolds with decreasing temperature as can be observed by the reappearance of the same secondary structural elements present in the native protein. In fact, at the end of the cooling process the spectrum is almost identical to that observed at 20 °C before heating, implying that the thermal unfolding−refolding process of AGP is reversible. This is in accordance with several other reports stating the thermal reversibility of AGP (*10*, *11*, *14*, *16*). The β-sheet bands at 1682.4 and 1629.8 cm^{-1} in the refolded AGP are not at the same frequencies as the native protein because AGP has undergone complete solvent exchange during protein unfolding. In addition, a band at 1645.5 cm^{-1} corresponding to unordered structures can be observed. Most probably this band could not be detected in the native protein because it was concealed by the band at 1634.4 cm^{-1}. The secondary structure content of AGP was then calculated on the deconvoluted spectrum of refolded AGP by the curve fitting method (*22*). The estimated secondary structure content revealed 50.3% β-sheets, 10.7% α-helices, 26.7% unordered structures, and 12.1% turns. These values are similar to those predicted by least-squares analysis of the amide I band made on native AGP by Kopecky et al., thus confirming the full reversibility of denatured AGP (*16*).

To better visualize conformational changes taking place during thermal unfolding of AGP, difference absorbance spectra from 20 to 90 °C were plotted (Figure 3A). Each difference spectrum allows the monitoring of small changes and is obtained by subtracting the spectrum recorded at the lower temperature from the one recorded 5 °C higher. Negative or positive bands in the amide I′ region reflect protein denaturation while adjacent positive and negative bands of similar intensities are indicative of band shifts in the two original absorbance spectra (*17*, *40*, *41*). The plot shows that in the 20−50 °C temperature range no appreciable changes can be observed, except for the small negative band at 1625 cm^{-1} corresponding to the disappearance of β-edge structures. Then, in the 50−65 °C temperature range negative and positive adjacent bands of similar intensities appear (1691−1682 and 1637−1626 cm^{-1}). These bands together with the absence of negative bands in the amide I′ region confirm that β-sheet structures experience solvent exchange and not denaturation in this range of temperature. This phenomenon is only possible if β-sheets become more exposed to the solvent (^2H_2O), thus allowing the protein to exchange residual amide hydrogens that had not exchanged during sample preparation. In fact, additional $^1H/^2H$ exchange is supported by the appearance of the negative 1545 cm^{-1} band (residual amide II band) in the 55−50, 60−55, and 65−60 °C difference spectra. These observations are indicative of a less folded state in which secondary structure elements are maintained. Above 65 °C the plots show that the protein begins to lose its secondary structures, as observed by the presence of two negative peaks, a small one at 1684 cm^{-1} and a large one at 1629 cm^{-1}, and a positive peak at

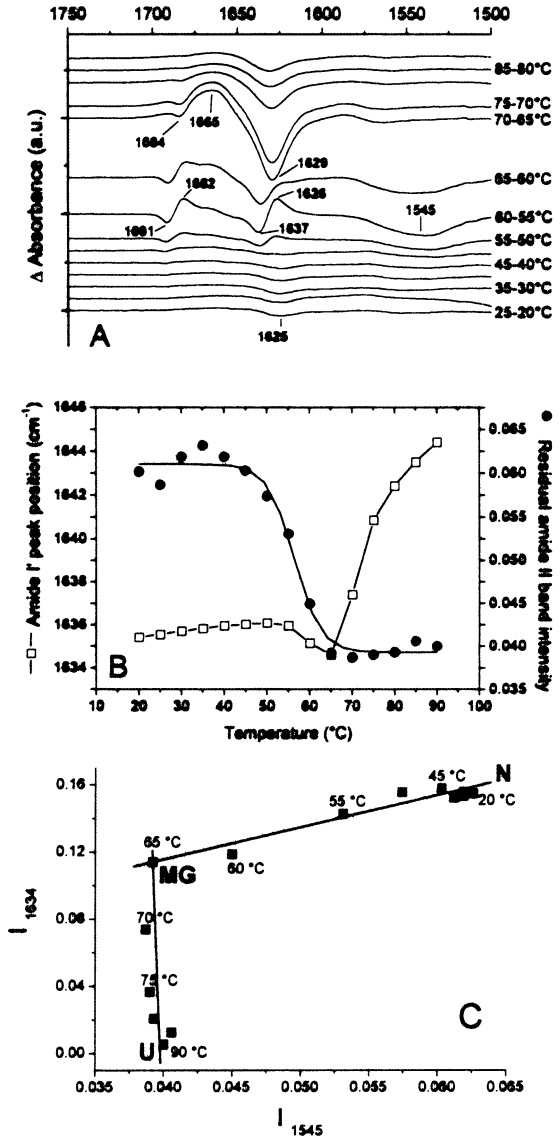

FIGURE 3: Difference spectra of AGP in the 20−90 °C temperature range (panel A), plot of the amide I′ peak position and of the residual amide II band intensity as a function of temperature (panel B), and phase diagram representing unfolding of AGP induced by temperature (panel C). Panel A: Each trace is obtained by subtracting the absorbance spectrum recorded at the lower temperature from the one recorded at the temperature 5 °C higher. Panel B: Monitoring of the position of the amide I′ peak (□) and of the intensity of the residual amide II band (●) vs temperature. The continuous line of the residual amide II band intensity curve represents the sigmoid fit based on the experimental points; its $T_{1/2}$ corresponds to 56.4 °C. Panel C: Each straight line represents an all-or-none transition between two conformers, denoted as N (native), MG (molten globule), and U (unfolded). Temperature values are indicated in the vicinity of the $I(\lambda_1)$ vs $I(\lambda_2)$ points (■).

1665 cm^{-1} corresponding to loss of β-sheet structures and formation of turns/bends, respectively. Maximum denaturation is observed between 65 and 75 °C. These difference spectra analyses further support the data reported and commented in Figure 2A.

AGP thermal unfolding can also be detected by monitoring the amide I′ peak position and the residual amide II band intensity as a function of temperature (Figure 3B). The amide I′ peak position curve shows a first transition between 55 and 65 °C, reflecting the β-sheet band shift observed in Figures 3A and 2A. Then a second transition occurs between

65 and 90 °C, which rapidly increases between 65 and 75 °C, reflecting protein denaturation. The residual amide II band intensity curve tracks solvent exchange of AGP with increasing temperature. From the curve one can deduce that exchange takes place between 50 and 65 °C and that from 65 °C onward protein solvent exchange is complete. This curve has a $T_{1/2}$ of 56.4 °C that coincides with the onset of the first transition of the amide I′ peak position. This demonstrates the correlation between $^1H/^2H$ exchange and β-sheet downshift. The end of solvent exchange also correlates well with the onset of protein denaturation, supporting the data described for Figure 3A.

Figure 3C represents the thermal unfolding of AGP using the phase diagram method of FT-IR. Using this multiparametric approach, we can validate that the temperature-induced unfolding of AGP involves one intermediate state. As can be seen from the diagram, this consists of two linear parts corresponding to 20−65 and 65−90 °C, indicating that the unfolding of AGP follows a three-state model: the native state (N) → the intermediate state (a less folded state, MG) → the unfolded state (U). In other words, the conformational transition between the native state and the intermediate state of this protein occurs in the temperature range of 20−65 °C, and the transition between the intermediate and the unfolded state occurs between 65 and 90 °C.

2D-IR COS Analysis of the Protein Unfolding Process. For a detailed analysis on the thermal behavior of AGP, generalized 2D-IR correlation spectroscopy on the infrared spectra obtained at different temperatures was applied. With this analysis two kinds of correlation spectra, synchronous and asynchronous, are generated from a set of dynamic spectra calculated from perturbation-induced dynamic fluctuations of spectroscopic signals (*42*−*46*). A synchronous spectrum represents the simultaneous or coincidental changes in spectral intensities measured at two discrete and independent wavenumbers, ν_1 and ν_2 (on *x*- and *y*-axes, respectively). An asynchronous spectrum represents sequential or unsynchronized changes of spectral intensities measured at ν_1 and ν_2 (*24*). Autopeaks are present only on the diagonal of a synchronous map while cross-peaks are present in either synchronous or asynchronous maps at the off-diagonal positions and they can be positive or negative. The sign of synchronous cross-peaks becomes positive if the spectral intensities at corresponding wavenumbers are either increasing or decreasing together as a function of temperature. Negative synchronous cross-peaks indicate that one of the spectral intensities is increasing while the other is decreasing. The sign of asynchronous cross-peaks becomes positive if the intensity change at ν_1 occurs predominantly before ν_2. On the other hand, it becomes negative if the change occurs after ν_2. This rule is reversed if the synchronous cross-peak at ν_1 and ν_2 is negative (*24*, *47*).

Figure 4 depicts the contour map representation of the synchronous and asynchronous spectra of AGP, generated from temperature-perturbed IR spectra in the 20−65 °C temperature interval. The synchronous spectrum is dominated by seven autopeaks: 1518, 1545, 1629, 1637, 1665, 1682, and 1691 cm^{-1} corresponding to tyrosine, residual amide II, β-sheets, β-sheets, turns/bends, β-sheets, and β-sheets, respectively. The 1637, 1682, and 1691 cm^{-1} ones are more intense, showing that these bands change markedly in this range of temperature. The description of all cross-peaks in the synchronous and asynchronous spectra is summarized in Tables 1 and 2. For instance, the positive cross-peak at 1545 vs 1637 cm^{-1} represents the correlation between

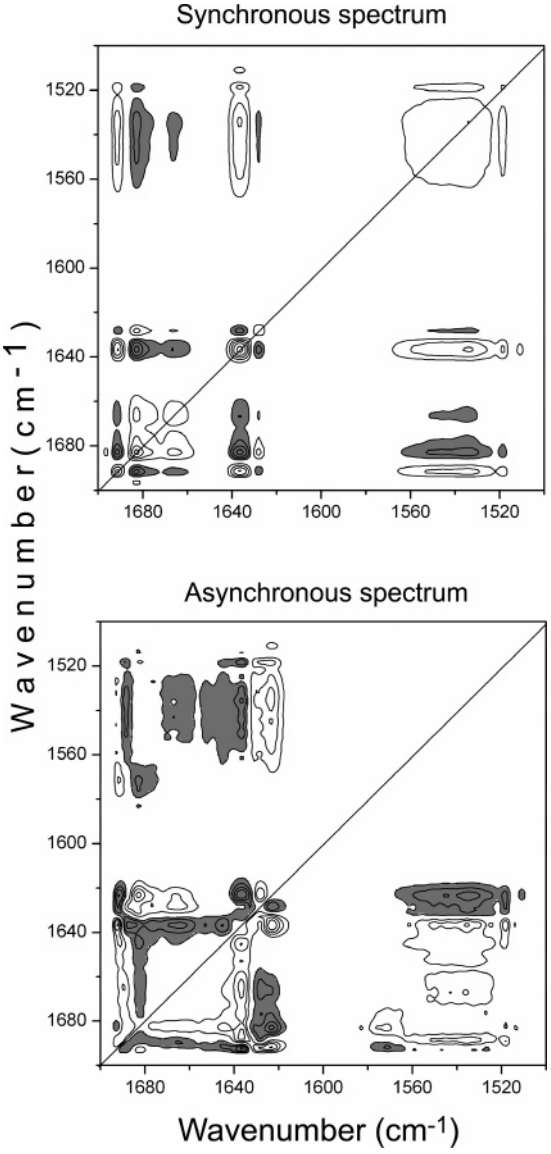

FIGURE 4: Synchronous and asynchronous 2D-IR COS spectra of AGP. Contour maps were generated using deconvoluted spectra in the 20−65 °C temperature range. Negative cross-peaks are represented in gray while positive cross-peaks are represented in white. Multiple lines represent intense peaks.

Table 1: Schematic Representation of the Synchronous Spectrum of AGP Obtained Using Deconvoluted Spectra from 20 to 65 °C in the 1700−1500 cm^{-1} Spectral Range[a]

1518↓							A
1545↓						A	+
1629↑					A	−	
1637↓				A	−	+	+
1665↑			A	−	+	−	
1682↑		A	+	−	+	−	−
1691↓	A	−	−	+	−	+	+
cm^{-1}	1691↓	1682↓	1665↓	1637↓	1629↑	1545↓	1518↓

[a] Peaks in the lower part of the synchronous spectrum of AGP (Figure 4) are shown. Autopeaks are represented by letters (A). Positive and negative cross-peaks are represented by the signs (+) and (−), respectively, and they are described by ν_1 (latter row) and ν_2 (first column). The symbols (↑) and (↓) indicate the increase and decrease in peak intensity, respectively.

Table 2: Schematic Representation of the Asynchronous Spectrum of AGP Obtained Using Deconvoluted Spectra from 20 to 65 °C in the 1700−1500 cm^{-1} Spectral Range[a]

1518↓									
1545↓									
1623↓								−a	−a
1629↑							−b		
1637↓							+b	+b	+b
1645↑					+a				
1665↑					+a	−a	−b	+a	
1682↑				+b	+a		−b		
1691↓			−b	−b	−a		+b		
cm^{-1}	1691↓	1682↑	1665↑	1645↑	1637↓	1629↓	1623↑	1545↓	1518↓

[a] Peaks in the lower part of the asynchronous spectrum of AGP (Figure 4) are shown. They are described by ν_1 (latter row) and ν_2 (first column). The signs (+) and (−) represent positive and negative peaks, respectively. The letters (a) and (b) indicate that the intensity change at ν_1 occurs predominantly after and before ν_2, respectively. The symbols (↑) and (↓) indicate the increase and decrease in peak intensity, respectively.

residual amide II and the 1637 cm^{-1} β-sheet bands, whose intensities both decrease with increasing temperature. On the other hand, the negative cross-peak at 1545 vs 1629 cm^{-1} shows that the residual amide II and the 1629 cm^{-1} β-sheet bands decrease and increase, respectively. In the asynchronous spectrum, the positive cross-peak at 1545 vs 1637 cm^{-1} shows that the residual amide II band decreases before the 1637 cm^{-1} β-sheet band does while the negative cross-peak at 1545 vs 1623 cm^{-1} means that the residual amide II band decreases after the 1623 cm^{-1} β-sheet band does. On analyzing synchronous and asynchronous maps, it is possible to obtain the succession of spectral intensity changes associated with secondary structural elements: that is, the sequence of thermal unfolding events (*24*, *31*). The interpretation of the 2D-IR COS data for AGP revealed the following sequence of events in the 20−65 °C temperature interval: [1623 cm^{-1} ↓ (β-edge), 1645 cm^{-1} ↑ (unordered)]; → [1665 cm^{-1} ↑ (turns/bends)]; → [1518 cm^{-1} ↓ (tyrosine), 1545 cm^{-1} ↓ (residual amide II)]; → [1691 cm^{-1} ↓ (β-sheets), 1682 cm^{-1} ↑ (β-sheets)]; → [1637 cm^{-1} ↓ (β-sheets), 1629 cm^{-1} ↑ (β-sheets)], where the arrows (↓ and ↑) stand for decrease and increase, respectively, in band intensity. The events in square brackets occur simultaneously. The data indicate that as temperature increases the outer β-strands (β-edge) of AGP break down forming unordered structures. This event is followed by an increase in turns/bends. Then, decreases in residual amide II and tyrosine bands reflect the beginning of $^1H/^2H$ exchange of AGP. In fact, the subsequent events are the simultaneous decrease of the 1691 cm^{-1} and increase of the 1682 cm^{-1} bands, followed by the concomitant decrease of the 1637 cm^{-1} and increase of the 1629 cm^{-1} bands. These shifts can only be explained if the protein's structure relaxes, leading to the exposure of β-sheets residing in the protein core that now become exposed to the solvent. In fact, no major secondary structure changes were detected except for the initial loss in the outer β-strands. Synchronous and asynchronous spectra of AGP in the 60−95 °C temperature range were also generated. In the synchronous spectrum one intense autopeak at 1629 cm^{-1} and a weak one at 1665 cm^{-1} were observed (data not shown). The first autopeak corresponds to the loss of β-sheet structures while the second one is generated by the increase in turns/bends. The asynchronous spectrum showed a noisy pattern where out-of-phase cross-peaks were poorly defined, indicating the

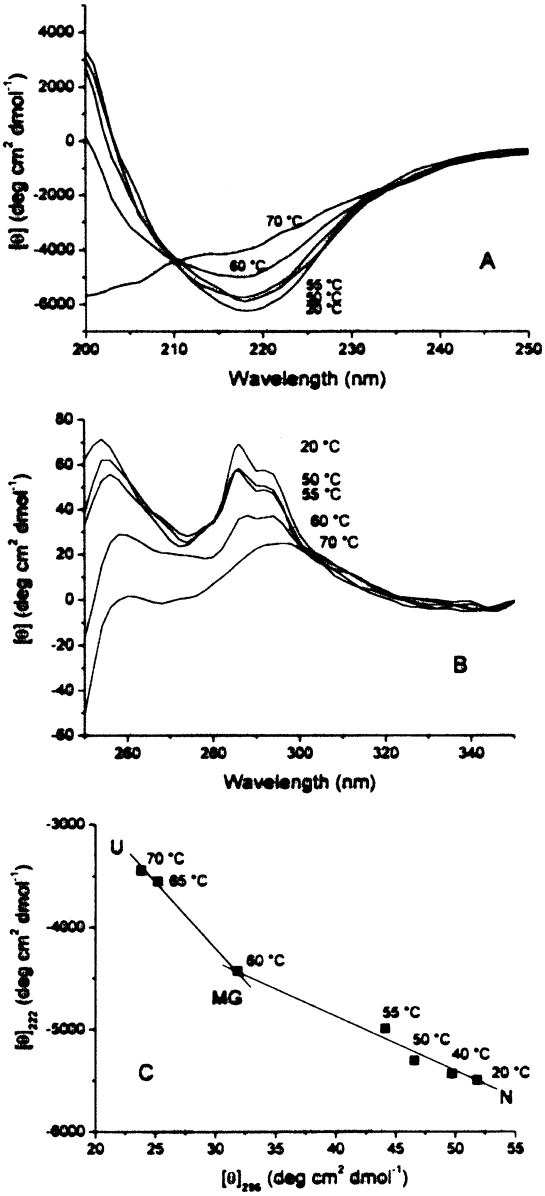

FIGURE 5: Far- (panel A) and near- (panel B) UV CD spectra of AGP in the 20−70 °C temperature range and phase diagram representing unfolding of AGP induced by temperature based on near/far-UV CD spectra (panel C). Panel A: CD spectra of 8 μM AGP in 20 mM phosphate buffer (pH 7.4) as a function of temperature recorded in the 200−250 nm region. Panel B: CD spectra of 20 μM AGP in 20 mM phosphate buffer (pH 7.4) as a function of temperature recorded in the 250−350 nm region. Panel C: Each straight line represents an all-or-none transition between two conformers, denoted as N (native), MG (molten globule), and U (unfolded). Temperature values are indicated in the vicinity of the $[\theta]_{222}$ vs $[\theta]_{296}$ points (■).

simultaneous occurrence of the events (*48*). Therefore, in the 60−95 °C temperature range, the unfolding of β-sheets, together with the formation of turns/bends, is the only event detectable during protein denaturation by 2D-IR COS. All of the information obtained in the synchronous and asynchronous spectra were consistent with and confirm the comments made on the second derivative and difference absorbance spectra of AGP.

Thermal Unfolding of AGP from CD Spectra. The effect of temperature on the CD spectra of AGP is illustrated in Figure 5A,B. One can observe that the far-UV spectra (Figure 5A) recorded between 20 and 55 °C show only minor spectral

changes in the secondary structure of AGP in accordance with the FT-IR data. Accordingly, the shape of the CD spectra remains virtually the same in this temperature range. However, at 60 °C there is a remarkable change in the shape of the CD spectrum, which shows a decrease in negative ellipticity around 222 nm and a decrease in positive ellipticity around 200 nm, suggesting loss in secondary structure. At 70 °C the spectrum resembles the typical pattern of a random coil structure indicating that the protein has undergone considerable denaturation. The qualitative appearance of the CD spectra in the near-UV (Figure 5B) shows that at 50 and 55 °C there is a decrease in rigid tertiary structure as can be deduced from the decrease in positive ellipticity, implying that the protein experiences a more relaxed state. The loss in tertiary structure becomes remarkably evident at 60 °C where the spectrum closely resembles that recorded at 70 °C, the temperature at which the protein is completely devoid of its tertiary structure. From these data it would appear that AGP maintains considerable nativelike compactness and secondary structure well up to 55 °C whereas its tertiary structure experiences relaxation. These observations in the CD spectra suggest the presence of an intermediate folded state between 50 and 55 °C during CD thermal unfolding of AGP. This assumption was confirmed by applying the phase diagram method using the ellipticity at 222 nm vs that at 296 nm. As can be seen from Figure 5C, this consists of two linear parts corresponding to 20−60 and 60−70 °C, indicating that the unfolding of AGP follows a three-state model, thus confirming the FT-IR data described in Figure 3. However, the discrepancies between the transition temperatures observed using FT-IR and CD spectroscopies are likely ascribed to the different experimental conditions employed (protein concentration, sample volume, etc.) and the different sensitivity of the two techniques for detecting protein structures as previously reported (*49*).

DISCUSSION

From the results presented in this study using the FT-IR technique combined with 2D-IR correlation spectroscopy and CD spectroscopy for monitoring AGP's conformational properties at definite temperatures, an interesting aspect has emerged. This is the formation of a molten globule-like state, which is different from the native and the unfolded protein. This may be regarded as a more open, relaxed condition of the protein in which a significant amount of native secondary structure is retained but little tertiary folds are present due to loosening of the network of the hydrogen bonds. The increased flexibility of the side chains and of the backbone leads to an influx of water, so that the molten globule state is rather highly hydrated (*50*, *51*). This lends some stability to the protein, which by its open, more flexible nature allows more surface for water interactions. This relaxation of the tertiary structure and the existence of water inside the globule have been demonstrated by NMR (*52*−*54*) and $^1H/^2H$ exchange techniques (*55*, *56*) and more recently by FT-IR spectroscopy (*17*, *31*, *57*, *58*). In fact, the peculiar characteristics of the molten globule fit with our findings of a further $^1H/^2H$ exchange in AGP between 55 and 65 °C as observed in the second derivative and difference spectra, and that corresponds to the first transition in the amide I′ peak position curve. In addition, within this temperature range no significant loss in secondary structure of the protein prior to denaturation was observed. The discrepancy in the temperature range at which the molten globule was observed with CD spectroscopy may be explained by the different experimental conditions employed as well as by the difference in sensitivity of the two techniques (*49*). The phase diagram of FT-IR and CD showing two linear parts that represent a three-state model and 2D-IR COS analysis revealing the sequence of secondary structures events also confirmed the formation of this less folded state.

The finding that AGP experiences a temperature-induced molten globule-like state lends support to the proposal of other authors who hypothesized the formation of an intermediate transient state during thermal unfolding of AGP using other spectroscopic techniques. For instance, Rojo-Dominguez et al. detected an intermediate state in AGP by the appearance of unusual positive difference absorption bands in the 287−295 nm region, which occurred at lower temperatures than the common denaturation bands at 284 and 291 nm. They assumed that the formation of this state apparently involves a local conformational change that perturbs the environment of tryptophyl residues, without affecting the secondary structure of the protein as judged from circular dichroism spectra (*13*). Instead, in the calorimetric study of Halsall and Kirley, van't Hoff enthalpies around 1.22 were found which indicate that thermal unfolding of AGP departs from a two-state model. They suggested that the source of the apparent multistate behavior may lie in the existence of polypeptide variants, known to be present in AGP (*11*). We now demonstrate that AGP experiences a molten globule-like state which has been observed for a number of proteins under different conditions, including at low pH and/or high temperatures, at moderately low dielectric constant and in the presence of denaturants (*52*, *54*, *59*). It is important to underline that features of the molten globule state were not observed on analyzing FT-IR second derivative spectra during thermal cooling from 90 to 20 °C of AGP (Figure 2B). Indeed, by the time the protein has reached 90 °C it has entirely $^1H/^2H$ exchanged; hence detection of the formation of this intermediate state by monitoring the parameters previously used upon heating is no longer possible.

Another interesting aspect that has come out during the course of this study is that the FT-IR data of AGP during thermal denaturation are very similar to those observed for two other β-sheet-rich proteins, porcine odorant-binding protein (OBP) and thioredoxin from *Escherichia coli* and *Alicyclobacillus acidocaldarius*. In both of these proteins a molten globule-like state was detected (*17*, *31*). This suggests that FT-IR spectroscopy might be a very useful tool for identifying this intermediate state in small proteins rich in β-sheets because this can be revealed by monitoring the position and intensity of the main β-sheet bands. It is worth recalling that FT-IR spectroscopy shows a higher sensitivity in detecting β-sheets than α-helices. However, in the case of a protein with a low content of β-sheets, the detection of a molten globule state is probably much more difficult or not possible. Moreover, we analyzed the structure of small proteins. In the case of larger proteins, even with a high content of β-sheets but with different domains, it would be difficult to unambiguously assign changes in the characteristics of a β-sheet band to the formation of a molten globule-like state.

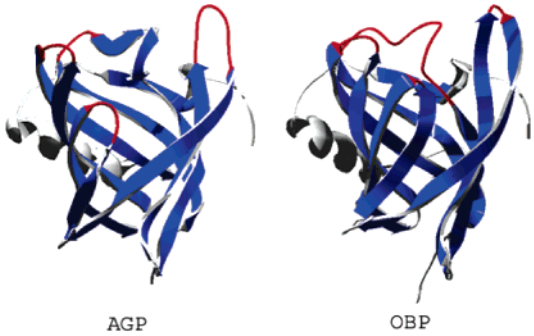

FIGURE 6: 3D structures of AGP and OBP. Ribbon molecular models (Swiss-PdbViewer) of the crystal structure of OBP (Protein Data Bank entry 1A3Y) and of the homology-modeled AGP using OBP as template. In both proteins the eight antiparallel strands of the conserved β-barrel structure are shown in blue. The four loops which are highly variable among the lipocalin family are colored in red, and the typical α-helix that is attached to the central β-barrel in all lipocalins, the N- and C-terminal peptide segments, and the loops at the closed end are shown in gray.

Interestingly, identical FT-IR deconvoluted and second derivative spectra of AGP and OBP were also noticed (*17*). Both AGP and OBP belong to a small subgroup of the lipocalin family, a large group of small extracellular proteins characterized by a highly conserved eight-stranded β-barrel structure despite lacking high sequence similarity (often well below 20%) (*1*). The fact that two proteins belonging to the same family have the same FT-IR spectral characteristics and show the same thermal unfolding behavior highlights the precision and reproducibility of the FT-IR technique. On account of the similarities in the FT-IR spectra of AGP with those of OBP, we attempted to achieve by homology modeling a 3D structure of AGP using OBP as template. OBP has been crystallized and its secondary structure previously calculated by us from its FT-IR spectra is in accordance with the values observed by X-ray diffraction (*17*). However, AGP has proved difficult to crystallize; hence its 3D structure is unknown. As can be observed in Figure 6, the 3D model of AGP is very similar to that of OBP. In both proteins one can spot the conserved β-barrel structure with one end typically open to the solvent providing access to the cavity. Interestingly, the secondary structure of AGP calculated from this 3D model (56% β-strand, 11.4% α-helix, and 27% unordered structures) is in strong agreement with the content estimated from the FT-IR deconvoluted spectrum of refolded AGP by the curve fitting method. This finding demonstrates that proteins which share almost identical FT-IR spectral characteristics and that behave similarly upon thermal denaturation also exhibit very similar 3D structures. Furthermore, the results demonstrate how FT-IR spectroscopy can be useful to estimate the secondary structure of proteins especially of those whose 3D structure has not yet been identified. Overall, this detailed FT-IR study contributes to understanding further the nature, the extent, and the sequence of the conformational changes surrounding the thermal stability of α_1-acid glycoprotein and highlights the utility of FT-IR spectroscopy for obtaining such information.

Other lipocalin proteins such as β-lactoglobulin and retinal-binding protein have also been shown to exhibit a molten globule state as a function of temperature and pH, respectively (*58*, *60*). Although the detection of this molten globule state has been observed under nonphysiological conditions (i.e., high temperatures, acidic pH), it nevertheless points out the propensity of these proteins to exist in this more relaxed state, which in a more physiological environment may have important implications. In fact, it has been suggested that the molten globule condition, probably favored by a β-barrel topology, may be important for a number of processes occurring in vivo, including the translocation of proteins through membranes, their folding, and degradation (*61*) as well as ligand release (*62*, *63*).

REFERENCES

1. Flower, D. R. (1996) The lipocalin protein family: structure and function, *Biochem. J. 318* (Part 1), 1−14.
2. Kute, T., and Westphal, U. (1976) Steroid-protein interactions. XXXIV. Chemical modification of alpha1-acid glycoprotein for characterization of the progesterone binding site, *Biochim. Biophys. Acta 420*, 195−213.
3. Fournier, T., Medjoubi, N. N., and Porquet, D. (2000) Alpha-1-acid glycoprotein, *Biochim. Biophys. Acta 1482*, 157−171.
4. Schmid, K., Kaufmann, H., Isemura, S., Bauer, F., Emura, J., Motoyama, T., Ishiguro, M., and Nanno, S. (1973) Structure of α_1-acid glycoprotein. The complete amino acid sequence, multiple amino acid substitutions, and homology with the immunoglobulins, *Biochemistry 12*, 2711−2724.
5. Kirley, T. L., Sprague, E. D., and Halsall, H. B. (1982) The binding of spin-labeled propranolol and spin-labeled progesterone by orosomucoid, *Biophys. Chem. 15*, 209−216.
6. Kremer, J. M., Wilting, J., and Janssen, L. H. (1988) Drug binding to human alpha-1-acid glycoprotein in health and disease, *Pharmacol. Rev. 40*, 1−47.
7. Israili, Z. H., and Dayton, P. G. (2001) Human alpha-1-glycoprotein and its interactions with drugs, *Drug Metab. Rev. 33*, 161−235.
8. Williams, J. P., Weiser, M. R., Pechet, T. T., Kobzik, L., Moore, F. D., Jr., and Hechtman, H. B. (1997) alpha 1-Acid glycoprotein reduces local and remote injuries after intestinal ischemia in the rat, *Am. J. Physiol. 273*, G1031−G1035.
9. Hochepied, T., Berger, F. G., Baumann, H., and Libert, C. (2003) Alpha(1)-acid glycoprotein: an acute phase protein with inflammatory and immunomodulating properties, *Cytokine Growth Factor Rev. 14*, 25−34.
10. Busby, T. F., and Ingham, K. C. (1986) Thermal stability and ligand-binding properties of human plasma alpha 1-acid glycoprotein (orosomucoid) as determined with fluorescent probes, *Biochim. Biophys. Acta 871*, 61−71.
11. Halsall, H. B., and Kirley, T. L. (1982) The denaturation of orosomucoid, *Arch. Biochem. Biophys. 216*, 392−399.
12. Hofbauerova, K., Kopecky, V., Jr., Sykora, J., and Karpenko, V. (2003) Thermal stability of the human blood serum acid alpha-(1)-glycoprotein in acidic media, *Biophys. Chem. 103*, 25−33.
13. Rojo-Dominguez, A., Zubillaga-Luna, R., and Hernandez-Arana, A. (1990) Unfolding behavior of human alpha 1-acid glycoprotein is compatible with a loosely folded region in its polypeptide chain, *Biochemistry 29*, 8689−8695.
14. Kodicek, M., Infanzon, A., and Karpenko, V. (1995) Heat denaturation of human orosomucoid in water/methanol mixtures, *Biochim. Biophys. Acta 1246*, 10−16.
15. Jirgensons, B. (1978) Circular dichroism studies on the effects of ethanol on the conformation of alpha1-acid glycoprotein, alpha1-antitrypsin, deoxyribonuclease, pepsinogen, soybean trypsin inhibitor and unfolded ribonucleases, *Biochim. Biophys. Acta 534*, 123−131.
16. Kopecky, V., Jr., Ettrich, R., Hofbauerova, K., and Baumruk, V. (2003) Structure of human alpha1-acid glycoprotein and its high-affinity binding site, *Biochem. Biophys. Res. Commun. 300*, 41−46.
17. Paolini, S., Tanfani, F., Fini, C., Bertoli, E., and Paolo, P. (1999) Porcine odorant-binding protein: structural stability and ligand affinities measured by Fourier-transform infrared spectroscopy and fluorescence spectroscopy, *Biochim. Biophys. Acta 1431*, 179−188.
18. Salomaa, P., Schaleger, L. L., and Long, F. A. (1964) Solvent deuterium isotope effects on acid−base equilibria, *J. Am. Chem. Soc. 86*, 1−7.

19. Tanfani, F., Galeazzi, T., Curatola, G., Bertoli, E., and Ferretti, G. (1997) Reduced beta-strand content in apoprotein B-100 in smaller and denser low-density lipoprotein subclasses as probed by Fourier-transform infrared spectroscopy, *Biochem. J. 322* (Part 3), 765−769.
20. Osborne, H. B., and Nabedryk-Viala, E. (1982) Infrared measurement of peptide hydrogen exchange in rhodopsin, *Methods Enzymol. 88*, 676−680.
21. Meersman, F., Smeller, L., and Heremans, K. (2002) Comparative Fourier transform infrared spectroscopy study of cold-, pressure-, and heat-induced unfolding and aggregation of myoglobin, *Biophys. J. 82*, 2635−2644.
22. Banuelos, S., Arrondo, J. L., Goni, F. M., and Pifat, G. (1995) Surface-core relationships in human low-density lipoprotein as studied by infrared spectroscopy, *J. Biol. Chem. 270*, 9192−9196.
23. Zolese, G., Falcioni, G., Bertoli, E., Galeazzi, R., Wozniak, M., Wypych, Z., Gratton, E., and Ambrosini, A. (2000) Steady-state and time-resolved fluorescence of albumins interacting with N-oleylethanolamine, a component of the endogenous N-acylethanolamines, *Proteins 40*, 39−48.
24. Noda, I. (1993) Generalized two-dimensional correlation method applicable to infrared, Raman, and other types of spectroscopy, *Appl. Spectrosc. 47*, 1329−1336.
25. Noda, I., and Ozaki, Y. (2004) Generalized two-dimensional correlation spectroscopy, Wiley, New York.
26. Morita, S., Ozaki, Y., and Noda, I. (2001) Global phase angle description, *Appl. Spectrosc. 55*, 1618−1621.
27. Thomas, M., and Richardson, H. H. (2000) Moving-window two-dimensional correlation spectroscopy, *Vib. Spectrosc. 24*, 137−146.
28. Fabian, H., Mantsch, H. H., and Schultz, C. P. (1999) Two-dimensional IR correlation spectroscopy: sequential events in the unfolding process of the lambda cro-V55C repressor protein, *Proc. Natl. Acad. Sci. U.S.A. 96*, 13153−13158.
29. Lambert, C., Leonard, N., De Bolle, X., and Depiereux, E. (2002) ESyPred3D: Prediction of proteins 3D structures, *Bioinformatics 18*, 1250−1256.
30. Kuznetsova, I. M., Turoverov, K. K., and Uversky, V. N. (2004) Use of the phase diagram method to analyze the protein unfolding-refolding reactions: fishing out the "invisible" intermediates, *J. Proteome Res. 3*, 485−494.
31. Pedone, E., Bartolucci, S., Rossi, M., Pierfederici, F. M., Scire, A., Cacciamani, T., and Tanfani, F. (2003) Structural and thermal stability analysis of *Escherichia coli* and *Alicyclobacillus acidocaldarius* thioredoxin revealed a molten globule-like state in thermal denaturation pathway of the proteins: an infrared spectroscopic study, *Biochem. J. 373*, 875−883.
32. D'Auria, S., Scire, A., Varriale, A., Scognamiglio, V., Staiano, M., Ausili, A., Marabotti, A., Rossi, M., and Tanfani, F. (2005) Binding of glutamine to glutamine-binding protein from *Escherichia coli* induces changes in protein structure and increases protein stability, *Proteins 58*, 80−87.
33. Byler, D. M., and Susi, H. (1986) Examination of the secondary structure of proteins by deconvolved FTIR spectra, *Biopolymers 25*, 469−487.
34. Arrondo, J. L., Muga, A., Castresana, J., and Goni, F. M. (1993) Quantitative studies of the structure of proteins in solution by Fourier-transform infrared spectroscopy, *Prog. Biophys. Mol. Biol. 59*, 23−56.
35. Surewicz, W. K., and Mantsch, H. H. (1988) New insight into protein secondary structure from resolution-enhanced infrared spectra, *Biochim. Biophys. Acta 952*, 115−130.
36. Krimm, S., and Bandekar, J. (1986) Vibrational spectroscopy and conformation of peptides, polypeptides, and proteins, *Adv. Protein Chem. 38*, 181−364.
37. Chirgadze, Y. N., Fedorov, O. V., and Trushina, N. P. (1975) Estimation of amino acid residue side-chain absorption in the infrared spectra of protein solutions in heavy water, *Biopolymers 14*, 679−694.
38. Chirgadze, Y. N., and Nevskaya, N. A. (1976) Infrared spectra and resonance interaction of amide-I vibration of the antiparallel-chain pleated sheet, *Biopolymers 15*, 607−625.
39. Susi, H., Timasheff, S. N., and Stevens, L. (1967) Infrared spectra and protein conformations in aqueous solutions. I. The amide I band in H_2O and D_2O solutions, *J. Biol. Chem. 242*, 5460−5466.
40. Leonhard, M., and Mantele, W. (1993) Fourier transform infrared spectroscopy and electrochemistry of the primary electron donor in *Rhodobacter sphaeroides* and *Rhodopseudomonas viridis* reaction centers: vibrational modes of the pigments in situ and evidence for protein and water modes affected by P+ formation, *Biochemistry 32*, 4532−4538.
41. Banecki, B., Zylicz, M., Bertoli, E., and Tanfani, F. (1992) Structural and functional relationships in DnaK and DnaK756 heat-shock proteins from *Escherichia coli*, *J. Biol. Chem. 267*, 25051−25058.
42. Noda, I. (1990) Two-dimensional infrared (2D IR) spectroscopy: theory and applications, *Appl. Spectrosc. 44*, 550−561.
43. Ozaki, Y., and Noda, I. (1996) Potential of generalised two-dimensional correlation spectroscopy in the near infrared region, *J. Near Infrared Spectrosc. 4*, 85−99.
44. Noda, I., Liu, Y., Ozaki, Y., and Czarnecki, M. A. (1995) Two-dimensional Fourier transform near-infrared correlation spectroscopy studies of temperature-dependent spectral variations of oleyl alcohol, *J. Phys. Chem. 99*, 3068−3073.
45. Noda, I., Liu, Y., and Ozaki, Y. (1996) Two-dimensional correlation spectroscopy study of temperature-dependent spectral variations of *N*-methylacetamide in the pure liquid state. 2. Two-dimensional Raman and infrared-Raman heterospectral analysis, *J. Phys. Chem. 100*, 8674−8680.
46. Noda, I., Liu, Y., and Ozaki, Y. (1996) Two-dimensional correlation spectroscopy study of temperature-dependent spectral variations of *N*-methylacetamide in the pure liquid state. 1. Two-dimensional infrared analysis, *J. Phys. Chem. 100*, 8665−8673.
47. Filosa, A., Wang, Y., Ismail, A. A., and English, A. M. (2001) Two-dimensional infrared correlation spectroscopy as a probe of sequential events in the thermal unfolding of cytochromes *c*, *Biochemistry 40*, 8256−8263.
48. Paquet, M. J., Laviolette, M., Pezolet, M., and Auger, M. (2001) Two-dimensional infrared correlation spectroscopy study of the aggregation of cytochrome *c* in the presence of dimyristoylphosphatidylglycerol, *Biophys. J. 81*, 305−312.
49. D'Auria, S., Alfieri, F., Staiano, M., Palella, F., Rossi, M., Scire, A., Tanfani, F., Bertoli, E., Grycznyski, Z., and Lakowicz, J. R. (2004) Structural and thermal stability characterization of *Escherichia coli* D-galactose/D-glucose-binding protein, *Biotechnol. Prog. 20*, 330−337.
50. Kharakoz, D. P., and Bychkova, V. E. (1997) Molten globule of human alpha-lactalbumin: hydration, density, and compressibility of the interior, *Biochemistry 36*, 1882−1890.
51. Onuchic, J. N., Nymeyer, H., Garcia, A. E., Chahine, J., and Socci, N. D. (2000) The energy landscape theory of protein folding: insights into folding mechanisms and scenarios, *Adv. Protein Chem. 53*, 87−152.
52. Kuwajima, K. (1996) The molten globule state of alpha-lactalbumin, *FASEB J. 10*, 102−109.
53. Mora-Gutierrez, A., Kumosinski, T. F., and Farrell, H. M. J. (1997) Oxygen-17 nuclear magnetic resonance studies of bovine and caprine casein hydration and activity in deuterated sugar solutions, *J. Agric. Food Chem. 45*, 4545−4553.
54. Englander, S. W. (2000) Protein folding intermediates and pathways studied by hydrogen exchange, *Annu. Rev. Biophys. Biomol. Struct. 29*, 213−238.
55. Dolgikh, D. A., Abaturov, L. V., Bolotina, I. A., Brazhnikov, E. V., Bychkova, V. E., Gilmanshin, R. I., Lebedev, Yu. O., Semisotnov, G. V., Tiktopulo, E. I., Ptitsyn, O. B., et al. (1985) Compact state of a protein molecule with pronounced small-scale mobility: bovine alpha-lactalbumin, *Eur. Biophys. J. 13*, 109−121.
56. Dolgikh, D. A., Gilmanshin, R. I., Brazhnikov, E. V., Bychkova, V. E., Semisotnov, G. V., Venyaminov, S., and Ptitsyn, O. B. (1981) Alpha-lactalbumin: compact state with fluctuating tertiary structure?, *FEBS Lett. 136*, 311−315.
57. Dong, A., and Lam, T. (2005) Equilibrium titrations of acid-induced unfolding-refolding and salt-induced molten globule of cytochrome *c* by FT-IR spectroscopy, *Arch. Biochem. Biophys. 436*, 154−160.
58. Qi, X. L., Holt, C., McNulty, D., Clarke, D. T., Brownlow, S., and Jones, G. R. (1997) Effect of temperature on the secondary structure of beta-lactoglobulin at pH 6.7, as determined by CD and IR spectroscopy: a test of the molten globule hypothesis, *Biochem. J. 324* (Part 1), 341−346.
59. Bychkova, V. E., Dujsekina, A. E., Klenin, S. I., Tiktopulo, E. I., Uversky, V. N., and Ptitsyn, O. B. (1996) Molten globule-like

state of cytochrome *c* under conditions simulating those near the membrane surface, *Biochemistry 35*, 6058−6063.
60. Bychkova, V. E., Berni, R., Rossi, G. L., Kutyshenko, V. P., and Ptitsyn, O. B. (1992) Retinol-binding protein is in the molten globule state at low pH, *Biochemistry 31*, 7566−7571.
61. Bychkova, V. E., Pain, R. H., and Ptitsyn, O. B. (1988) The "molten globule" state is involved in the translocation of proteins across membranes?, *FEBS Lett. 238*, 231−234.
62. Jeffrey, P. D., Bewley, M. C., MacGillivray, R. T., Mason, A. B., Woodworth, R. C., and Baker, E. N. (1998) Ligand-induced conformational change in transferrins: crystal structure of the open form of the N-terminal half-molecule of human transferrin, *Biochemistry 37*, 13978−13986.
63. Nishi, K., Maruyama, T., Halsall, H. B., Handa, T., and Otagiri, M. (2004) Binding of alpha1-acid glycoprotein to membrane results in a unique structural change and ligand release, *Biochemistry 43*, 10513−10519.

BI051512Z